

# An adaptive planewave method for electronic structure calculations

Beilei Liu\*, Huajie Chen†, Geneviève Dusson‡, Jun Fang§, Xingyu Gao¶

## Abstract

We propose an adaptive planewave method for eigenvalue problems in electronic structure calculations. The method combines *a priori* convergence rates and accurate *a posteriori* error estimates into an effective way of updating the energy cut-off for planewave discretizations, for both linear and nonlinear eigenvalue problems. The method is *error controllable* for linear eigenvalue problems in the sense that for a given required accuracy, an energy cut-off for which the solution matches the target accuracy can be reached efficiently. Further, the method is particularly promising for nonlinear eigenvalue problems in electronic structure calculations as it shall reduce the cost of early iterations in self-consistent algorithms. We present some numerical experiments for both linear and nonlinear eigenvalue problems. In particular, we provide electronic structure calculations for some insulator and metallic systems simulated with Kohn–Sham density functional theory (DFT) and the projector augmented wave (PAW) method, illustrating the efficiency and potential of the algorithm.

## Contents

<b>1</b>	<b>Introduction</b>	<b>2</b>
<b>2</b>	<b>Linear eigenvalue problems</b>	<b>4</b>
2.1	Schrödinger-type equations . . . . .	4
2.2	Planewave discretization . . . . .	5
2.3	<i>A priori</i> error estimate . . . . .	5
2.4	<i>A posteriori</i> error estimate . . . . .	6
<b>3</b>	<b>Adaptive algorithm for linear problems</b>	<b>7</b>

---

\*beilei@mail.bnu.edu.cn. School of Mathematical Sciences, Beijing Normal University, No.19, Xijiekouwai Street, Beijing 100875, China.

†chen.huajie@bnu.edu.cn. School of Mathematical Sciences, Beijing Normal University, No.19, Xijiekouwai Street, Beijing 100875, China.

‡genevieve.dusson@math.cnrs.fr. Laboratoire de Mathématiques de Besançon, UMR CNRS 6623, Université Bourgogne Franche-Comté, 16 route de Gray, 25030 Besançon, France

§fang\_jun@iapcm.ac.cn. Institute of Applied Physics and Computational Mathematics, Fenghao East Road 2, Beijing 100094, China.

¶gao\_xingyu@iapcm.ac.cn. Laboratory of Computational Physics, Institute of Applied Physics and Computational Mathematics, Beijing 100088, China.

<b>4</b>	<b>Applications to nonlinear eigenvalue problems</b>	<b>10</b>
4.1	Kohn–Sham equations . . . . .	11
4.2	Adaptive algorithm for nonlinear problems . . . . .	12
<b>5</b>	<b>Numerical experiments</b>	<b>14</b>
5.1	Tests of principle . . . . .	14
5.2	Tests on PAW Kohn–Sham equations . . . . .	16
<b>6</b>	<b>Conclusions and perspectives</b>	<b>21</b>
	<b>Appendices</b>	<b>21</b>
	<b>Appendix A Evaluating the <i>a posteriori</i> error indicator</b>	<b>21</b>
A.1	A standard calculation . . . . .	21
A.2	A perturbation-based calculation . . . . .	23
	<b>Appendix B The PAW method</b>	<b>24</b>

# 1 Introduction

The electronic structure modelling of many-particle systems enables the investigation and prediction of properties of molecules and material systems and is used in different fields, such as in chemistry, materials science, biology, and nanosciences. Most of electronic structure models exhibit (possibly nonlinear) eigenvalue problems, in particular to compute the electronic ground state of a system within the Born–Oppenheimer approximation. To solve the underlying eigenvalue problems numerically, the planewave method is one of the most widely used discretization methods [34, 41, 45], and is employed in many packages, e.g. ABINIT [26], CASTEP [29], Quantum Espresso [25], and VASP [47]. By expressing the eigenfunction as a linear combination of planewave functions, this method has the following key advantages [45]. First, it is a natural discretization for periodic systems in materials science as the planewaves can match the translational symmetry of the systems perfectly. Second, the transformation from real to reciprocal space and vice versa can be done efficiently with fast Fourier transforms (FFTs), which makes the calculation of the elements of the Hamiltonian, the matrix that needs to be diagonalised, relatively simple. Third, as a spectral discretization method, the planewave method allows to achieve a spectral convergence rate when combined with pseudo-potential approximations [35].

A key issue in the planewave method is the choice of the energy cut-off, the parameter determining the number of basis functions. A larger cut-off will lead to more accurate results, but at the price of increasing the computational cost significantly. Therefore, it is important to choose an appropriate energy cut-off leading to the right accuracy while using as few planewaves as possible. Unfortunately, such a cut-off is *a priori* unknown. In practice, it is usually determined by testing the convergence of quantities of interest, such as the energy, the electron density, or the forces and stresses. Starting any simulation of a new system by a convergence test in order to determine a cut-off satisfying the above criterion can be quite demanding, as this requires to solve several times the same problem for different cut-offs.

The purpose of this paper is to present an elegant algorithm to determine an energy cut-off in an *a posteriori* way, so that the planewave approximation reaches the desired

accuracy, and avoids superfluous convergence-test computations. For Schrödinger-type linear eigenvalue problems, our algorithm relies on three important aspects: (i) an *a priori* error estimate that gives the decay rate of the discretization error; (ii) an *a posteriori* error estimate that gives guaranteed and asymptotically accurate error indicators; (iii) the strategy which predicts sensible energy cut-offs during the simulation. We further incorporate this algorithm into the self-consistent field (SCF) algorithm used to solve nonlinear eigenvalue problems, in particular the Kohn–Sham equations [33, 37] in Density Functional Theory (DFT) [31, 33], so that the energy cut-off is adapted along the iterations of the algorithm.

The idea of adapting the discretization on-the-fly has long been exploited, in particular in finite element methods, which have been extensively studied for both general elliptic equations [1, 5, 6, 17, 23, 28] and eigenvalue problems in quantum physics [2, 18, 20, 21, 22, 46, 48]. In adaptive methods, an efficient and reliable *a posteriori* error estimator is essential, in order to indicate how to improve the basis set, e.g. by modifying the energy cut-off for planewave methods. To this end, this work will use some guaranteed *a posteriori* error estimates presented in [11, 12, 13]. For planewave methods, there are only a handful of works devoted to the construction of the *a posteriori* error estimates and adaptive methods. We refer to [24] for *a posteriori* error estimates and [16, 30] for adaptive algorithms. To our best knowledge, there is very few efficient implementations of adaptive planewave algorithm for quantum eigenvalue problems [24], and no existing work for simulations of real systems with Kohn–Sham equations. The difference lies in that the planewaves are non-local basis functions, and the traditional local refinement techniques used in adaptive finite element discretizations cannot be applied straightforwardly.

As a major application of our algorithm, we carry out electronic structure calculations in the framework of Kohn–Sham DFT and the projector augmented-wave (PAW) method [7, 27, 35]. The PAW method is a very accurate and widely used method in electronic structure calculations, which has an elegant theoretical framework based on a linear transformation from the pseudo wave-functions to the real all-electron ones and then derives closed-form expressions for electronic densities, energy functionals, and forces in a consistent manner. This method has now been efficiently implemented in several simulation packages, including the well-known VASP and ABINIT codes, and widely applied in materials science, condensed matter physics, and quantum chemistry. In practical PAW calculations, a proper setting of the planewave cut-off for the pseudo wave-function to ensure numerical convergence is critical for obtaining meaningful simulation results.

The rest of the article is organized as follows. In Section 2, we focus on linear Schrödinger-type equations. We briefly discuss the planewave discretization, and available *a priori* and *a posteriori* error estimates. In Section 3, we propose two strategies to construct an adaptive algorithm for linear eigenvalue problems. In Section 4, the Kohn–Sham equations and the PAW method are presented, and the adaptive algorithm for linear eigenvalue problems is built into SCF iterations for the nonlinear eigenvalue problem. In Section 5, we perform some numerical experiments to show the validity and efficiency of our algorithms for linear and nonlinear eigenvalue problems. In particular, Kohn–Sham DFT calculations with the PAW method for some bulk systems are presented, including a diamond system and a metallic FCC aluminum system with a vanishing band gap. Finally, some concluding remarks are given in Section 6.

Throughout this paper, we shall use  $C$  to denote a generic positive constant which may stand for different values at its different occurrences but is independent of finite dimensional subspaces. The symbol  $\langle \cdot, \cdot \rangle$  denotes an abstract duality pairing between a Banach space and

its dual, and  $(\cdot, \cdot)$  denotes the inner product in the space  $L^2_{\#}(\Omega)$  introduced in Section 2.

## 2 Linear eigenvalue problems

In this section, we consider a Schrödinger-type equation, review the planewave discretization and discuss available *a priori* and *a posteriori* error estimates. We clarify at this point that, only the error estimates for linear eigenvalue problems are required and exploited for the adaptive planewave algorithms developed in this paper, for both Schrödinger-type and Kohn–Sham equations.

Let  $d \in \{1, 2, 3\}$  be the dimension of the system,  $\mathbb{L} = P\mathbb{Z}^d \subset \mathbb{R}^d$  be a Bravais lattice, where  $P \in \mathbb{R}^{d \times d}$  is a non-singular matrix. Let  $\Omega$  be a unit cell of the lattice  $\mathbb{L}$ , and  $\mathbb{L}'$  be the dual lattice of  $\mathbb{L}$ . We denote by  $e_{\mathbf{G}}(\mathbf{r}) = |\Omega|^{-1/2} e^{i\mathbf{G} \cdot \mathbf{r}}$  the planewave with wavevector  $\mathbf{G} \in \mathbb{L}'$ . The family  $\{e_{\mathbf{G}}\}_{\mathbf{G} \in \mathbb{L}'}$  forms an orthonormal basis set of  $L^2_{\#}(\Omega)$ , where

$$L^p_{\#}(\Omega) = \{u \in L^p_{\text{loc}}(\mathbb{R}^d) : u \text{ is } \mathbb{L}\text{-periodic}\}.$$

For all  $u \in L^2_{\#}(\Omega)$ , we have

$$u(\mathbf{r}) = \sum_{\mathbf{G} \in \mathbb{L}'} \hat{u}_{\mathbf{G}} e_{\mathbf{G}}(\mathbf{r}) \quad \text{with} \quad \hat{u}_{\mathbf{G}} = (u, e_{\mathbf{G}}) = |\Omega|^{-1/2} \int_{\Omega} u(\mathbf{r}) e^{-i\mathbf{G} \cdot \mathbf{r}} d\mathbf{r}.$$

We introduce the Sobolev spaces of real-valued  $\mathbb{L}$ -periodic functions for  $s \in \mathbb{R}$

$$H^s_{\#}(\Omega) = \left\{ u(\mathbf{r}) = \sum_{\mathbf{G} \in \mathbb{L}'} \hat{u}_{\mathbf{G}} e_{\mathbf{G}}(\mathbf{r}) : \forall \mathbf{G} \in \mathbb{L}', \hat{u}_{-\mathbf{G}} = \hat{u}_{\mathbf{G}}^*, \sum_{\mathbf{G} \in \mathbb{L}'} (1 + |\mathbf{G}|^2)^s |\hat{u}_{\mathbf{G}}|^2 < \infty \right\}.$$

### 2.1 Schrödinger-type equations

We consider a Schrödinger-type linear eigenvalue problem: Find  $(\lambda_i, \varphi_i) \in \mathbb{R} \times H^1_{\#}(\Omega)$ , such that  $\|\varphi_i\|_{L^2(\Omega)} = 1$  and

$$(-\Delta + V(\mathbf{r})) \varphi_i(\mathbf{r}) = \lambda_i \varphi_i(\mathbf{r}) \quad i = 1, 2, \dots, \quad (2.1)$$

where the potential  $V \in C^\infty(\mathbb{R}^d)$  and is  $\mathbb{L}$ -periodic. The smoothness assumption on the potential  $V$  is reasonable, since the planewave discretization is in practice often combined with smooth pseudo-potentials.

The weak form of (2.1) reads

$$a(\varphi_i, v) = \lambda_i (\varphi_i, v) \quad \forall v \in H^1_{\#}(\Omega) \quad i = 1, 2, \dots \quad (2.2)$$

with the bilinear form  $a(\cdot, \cdot) : H^1_{\#}(\Omega) \times H^1_{\#}(\Omega) \rightarrow \mathbb{R}$  given by

$$a(u, v) = \int_{\Omega} \nabla u \cdot \nabla v + \int_{\Omega} V u v. \quad (2.3)$$

Since the operator  $A := -\Delta + V$  is self-adjoint, bounded below with compact resolvent, there exists a non-decreasing sequence of eigenvalues  $\lambda_1 < \lambda_2 \leq \dots \leq \lambda_j \rightarrow +\infty$ , where the  $\lambda_j$ 's are repeated according to their multiplicity.

Up to shifting the operator by a positive constant, we can assume that all the eigenvalues are positive. We can further assume that  $V(\mathbf{r}) \geq 1$  ( $\forall \mathbf{r} \in \Omega$ ) for simplicity of illustration. Then it holds

$$a(v, v) \geq \|v\|_{H_{\#}^1(\Omega)}^2 \quad \forall v \in H_{\#}^1(\Omega),$$

and we can define the corresponding energy norm by  $\|\cdot\|_a := \sqrt{a(\cdot, \cdot)}$ .

## 2.2 Planewave discretization

Given an energy cut-off  $E_c > 0$ , we define the following finite dimensional space

$$X_{E_c}(\Omega) := \left\{ \sum_{\mathbf{G} \in \mathbb{L}', |\mathbf{G}|^2 \leq 2E_c} c_{\mathbf{G}} e_{\mathbf{G}}(\mathbf{r}), \forall \mathbf{G}, c_{-\mathbf{G}} = c_{\mathbf{G}}^* \right\}. \quad (2.4)$$

For  $v \in H_{\#}^s(\Omega)$ , the best approximation of  $v$  in  $X_{E_c}(\Omega)$  is  $\Pi_{E_c} v = \sum_{\mathbf{G} \in \mathbb{L}', |\mathbf{G}|^2 \leq 2E_c} \hat{v}_{\mathbf{G}} e_{\mathbf{G}}(\mathbf{r})$  for any  $H_{\#}^t$ -norm ( $t \leq s$ ). The more regularity  $v$  has, the faster this truncated series converge to  $v$ : For  $s, t \in \mathbb{R}_+$  satisfying  $t \leq s$ , we have that for each  $v \in H_{\#}^s(\Omega)$  (see e.g. [15]),

$$\|v - \Pi_{E_c} v\|_{H_{\#}^t(\Omega)} = \min_{w \in X_{E_c}} \|v - w\|_{H_{\#}^t(\Omega)} \lesssim E_c^{(t-s)/2} \|v\|_{H_{\#}^s(\Omega)}. \quad (2.5)$$

For simplicity of notation, we suppress for now the index for the considered eigenpair in the eigenvalue problem. We rewrite the linear problem (2.2) as

$$a(\varphi, v) = \lambda(\varphi, v) \quad \forall v \in H_{\#}^1(\Omega), \quad (2.6)$$

and present available *a priori* and *a posteriori* error estimates. We note that the following discussions are not restricted to a specific eigenpair, but require a gap between the considered eigenvalue and the surrounding ones.

Given an energy cut-off  $E_c$ , the planewave discretization is a Galerkin approximation of the eigenpairs of (2.6) within the finite dimensional subspace  $X_{E_c}(\Omega) \subset H_{\#}^1(\Omega)$ : Find  $(\lambda_{E_c}, \varphi_{E_c}) \in \mathbb{R} \times X_{E_c}(\Omega)$ , such that  $\|\varphi_{E_c}\|_{L_{\#}^2(\Omega)} = 1$  and

$$a(\varphi_{E_c}, v) = \lambda_{E_c}(\varphi_{E_c}, v) \quad \forall v \in X_{E_c}(\Omega). \quad (2.7)$$

## 2.3 A priori error estimate

An *a priori* estimate for the solutions  $(\lambda_{E_c}, \varphi_{E_c})$  of (2.7) can be found in [39, Theorems 2 and 3]. There exists a constant  $C > 0$  independent of  $E_c$ , such that

$$\|\varphi - \varphi_{E_c}\|_{H_{\#}^1(\Omega)} \leq C \inf_{\psi_{E_c} \in X_{E_c}} \|\varphi - \psi_{E_c}\|_{H_{\#}^1(\Omega)} \quad \text{and} \quad (2.8)$$

$$|\lambda - \lambda_{E_c}| \leq C \|\varphi - \varphi_{E_c}\|_{H_{\#}^1(\Omega)}^2. \quad (2.9)$$

Hence, if the eigenfunction  $\varphi$  is analytic, which we will assume in the following, then the approximation error decays exponentially as (see [15, Section 5.4, Eq. (5.4.5)])

$$\|\varphi - \varphi_{E_c}\|_{H_{\#}^1(\Omega)} \leq C e^{-c\sqrt{E_c}} \quad \text{and} \quad (2.10)$$

$$|\lambda - \lambda_{E_c}| \leq C e^{-\tilde{c}\sqrt{E_c}}. \quad (2.11)$$

with the constants  $C, c, \tilde{c} > 0$  independent of  $E_c$ . The above *a priori* error estimates not only guarantee that the error goes to zero as the energy cut-off increases, but also offer the speed of convergence of the approximate solutions to the exact one.

We observe from the numerical experiments (see Figure 5.1 in Section 5.1) that for the smooth tested potential, the error of planewave approximations decay exponentially fast with respect to  $\sqrt{E_c}$ , which matches the *a priori* error estimate in (2.10) and (2.11).

In Section 3, we will combine the *a priori* bounds (2.10) and (2.11) with the *a posteriori* bounds presented below in a linear regression strategy for determining good energy cut-offs.

**Remark 2.1.** *Analogous to the linear eigenvalue problem (2.6), some optimal a priori error estimates for nonlinear eigenvalue problems can be obtained [8, 9, 19].*

## 2.4 A posteriori error estimate

To develop an adaptive method, it is very useful to have *a posteriori* error estimators available. Unlike *a priori* error estimates, the goal of the *a posteriori* error estimates is to provide a computable bound on the error between the numerical approximation of the solution and the unknown exact solution. This bound should therefore be computable with the knowledge of the approximate solution and the parameters used for the computation only.

In this section, we review an *a posteriori* error estimator for the planewave approximation of the linear eigenvalue problem (2.1), which gives computable and asymptotically accurate approximate errors. This *a posteriori* error indicator was first introduced for simple eigenvalues for conforming finite element discretizations in [11], nonconforming methods in [12], and then extended to eigenvalue clusters in [13].

Let us denote  $H_{\#}^1(\Omega)$  by  $H$  and its dual by  $H'$  for simplicity of notations. Let  $(\lambda, \varphi) \in \mathbb{R} \times H$  be an eigenpair of (2.6) and  $(\lambda_{E_c}, \varphi_{E_c}) \in \mathbb{R} \times X_{E_c}(\Omega)$  be the corresponding planewave approximation with a given energy cut-off  $E_c$ . We define the residual  $\text{Res}(\lambda_{E_c}, \varphi_{E_c}) \in H'$  by

$$\langle \text{Res}(\lambda_{E_c}, \varphi_{E_c}), v \rangle_{H', H} = a(\varphi_{E_c}, v) - \lambda_{E_c}(\varphi_{E_c}, v) \quad \forall v \in H. \quad (2.12)$$

The idea of residual-based *a posteriori* error estimation is to estimate the error of the approximation by the dual norm of the residual in an appropriate Hilbert space. Note that the dual norm must be well chosen, otherwise the norm of the residual might not accurately represent the error or not even go to zero when the error goes to zero. To construct the *a posteriori* error estimator for the approximation  $(\lambda_{E_c}, \varphi_{E_c})$ , we consider the dual norm of the residual

$$\eta(\lambda_{E_c}, \varphi_{E_c}) := \|\text{Res}(\lambda_{E_c}, \varphi_{E_c})\|_{a'}, \quad (2.13)$$

where the dual norm (with respect to the energy norm  $\|\cdot\|_a$ ) is defined by

$$\|f\|_{a'} := \sup_{v \in H, v \neq 0} \frac{\langle f, v \rangle_{H', H}}{\|v\|_a} \quad \text{for } f \in H'.$$

For simplicity of notation, we will denote the residual and its dual norm by

$$\text{Res}_{E_c} = \text{Res}(\lambda_{E_c}, \varphi_{E_c}) \quad \text{and} \quad \eta_{E_c} = \eta(\lambda_{E_c}, \varphi_{E_c})$$

in the following. We have from [13] that if  $\lambda$  is a simple eigenvalue, there exists  $\alpha(E_c)$  with  $\alpha(E_c) \rightarrow 0$  as  $E_c \rightarrow \infty$  such that

$$0 \leq \lambda_{E_c} - \lambda \leq (1 + \alpha(E_c))\eta_{E_c}^2. \quad (2.14)$$

**Remark 2.2.** *So far, we have ignored the index  $j$  for the eigenpairs for simplicity of notation, but the error indicator for a specific eigenpair with index  $j$  can also be denoted by  $\eta_{E_c,j}$  for completeness. Thus, when considering multiple eigenpairs, the definition of  $\eta_{E_c}$  can be extended by taking the sum*

$$\eta_{E_c} := \left( \sum_{j \in J} \eta_{E_c,j}^2 \right)^{1/2},$$

where  $J$  is the set of indices of eigenpairs under consideration. Moreover, if the quantity of interest is not the sum of the eigenvalues, but a weighted sum, which happens to be the case in practice when fractional occupation numbers are in use, one can obtain error indicators on this quantity of interest by introducing corresponding weights in front of the individual error indicators  $\eta_{E_c,j}^2$ , as defined in Section 4.2.

**Remark 2.3.** *The above a posteriori error estimate can be directly generalized to linear operators with non-local potentials (see e.g. (4.3)).*

To evaluate the *a posteriori* error indicator (2.13), one needs to solve the infinite dimensional linear system (2.12) to compute the residual. A practical evaluation method is to restrict the trial function space and test function space in (2.12) to a finite dimensional subspace  $X_{E_g}(\Omega)$  (see definition (2.4)) with some cut-off  $E_g \gg E_c$ . We will then denote the computable error indicator by  $\eta_{E_c}^{E_g}$ , whose detailed calculations are presented in Appendix A. If  $E_g$  is proportional to  $E_c$ , then a standard calculation by solving the corresponding finite dimensional linear system will require a cost of  $\mathcal{O}(E_c^d)$ , and we refer to Appendix A.1 for the explanations.

In order to significantly reduce the cost of the error indicator, we can alternatively evaluate the residual via a perturbation-based method. The resulting error indicator will be denoted by  $\eta_{E_c}^{E_g,[k]}$  (with  $k = 1, 2$  the order of perturbation), whose cost is reduced to  $\mathcal{O}(E_c^{d/2})$ . We refer to Appendix A.2 for the derivation of this method and discussion of its computational cost.

### 3 Adaptive algorithm for linear problems

We are now ready to construct the adaptive algorithm for Schrödinger-type equations. The algorithm repeats the following procedure until the required accuracy is reached:

- (a) given the energy cut-off  $E_c$ , solve (2.7) to obtain the approximate eigenpair  $(\lambda_{E_c}, \varphi_{E_c})$ ;
- (b) compute the *a posteriori* error estimator  $\eta_{E_c}^{E_g}$  (or  $\eta_{E_c}^{E_g,[k]}$ ) from the approximation  $(\lambda_{E_c}, \varphi_{E_c})$  and a given  $E_g$ ;

(c) use some strategy to determine the new energy cut-off  $E_c^{\text{opt}}$ .

The step (a) is standard and the step (b) has been discussed in the previous section. To determine the energy cut-offs during the iterations, i.e. step (c), we propose two strategies. Note that to initialize the algorithm, we choose a relative small energy cut-off at the first step.

The first strategy relying on the known *a priori* spectral convergence rate (in Section 2.3) and the *a posteriori* error estimate (in Section 2.4) is presented in Strategy A. The idea is to perform a linear regression to predict the energy cut-off leading to a required accuracy. As an input for the linear regression, we use the  $k$ -th energy cut-offs and the *a posteriori* error indicators  $\{E_c^{(i)}, \eta_{E_c^{(i)}}^{E_g}\}_{0 \leq i \leq k}$ . We show in Figure 3.1 (a) a schematic plot of Strategy A.

---

**Strategy A:** Linear regression

---

**Given:** eigenvalue tolerance  $\varepsilon$ , energy cut-offs and error estimators  $\{E_c^{(i)}, \eta_{E_c^{(i)}}^{E_g}\}_{0 \leq i \leq k}$ .

1. Perform a linear regression to compute the linear function

$$\Theta(x) := \mathbf{LR} \left[ \left\{ \sqrt{E_c^{(i)}}, \log(\eta_{E_c^{(i)}}^{E_g}) \right\}_{0 \leq i \leq k} \right] (x). \quad (3.1)$$

2. Solve the following linear equation to obtain  $\bar{E}$

$$\Theta(\bar{E}) = \frac{1}{2} \log \varepsilon.$$

**Return:** Output energy cut-off  $E_{c,A}^{(k+1)} = \bar{E}$

---

In (3.1),  $\mathbf{LR}$  gives a linear function  $\Theta(x) = ax + b$ , where the coefficients  $a$  and  $b$  are determined by least squares as follows

$$\min_{a,b} \left\{ \sum_{0 \leq i \leq k} \left| a \sqrt{E_c^{(i)}} + b - \log(\eta_{E_c^{(i)}}^{E_g}) \right|^2 \right\}. \quad (3.2)$$

We observe from the numerical results in Section 5 that the strategy based on linear regression appears to be sharp in many cases, but sometimes overestimates the optimal energy cut-offs due to the fluctuation of the errors.

A second strategy is presented in Strategy B below. In this strategy, similar to the Dörlfer strategy, which is a widely used method in adaptive finite elements methods, the error indicator is seen as the sum of contributions from all wave vectors  $\mathbf{G}$  in the reciprocal space, and the energy cut-off is increased until sufficiently many  $\mathbf{G}$ 's are included so that the chosen tolerance is achieved. The error estimator (A.5) or (A.10) is used in the strategy to predict the new energy cut-off. We show in Figure 3.1 (b) a schematic plot of Strategy B. In the picture, the red circle and blue circles represent the cut-offs  $E_c$  and  $E_g$  respectively, and the *a posteriori* error estimate consists of the sum over all reciprocal lattice vectors that lie between these two circles. Strategy B determines the black circle, which is obtained such that the planewave vectors lie in between the red and black ones contribute to “most of the error” up to some given tolerance. In practice, (3.3) can be solved by using the bi-section or golden-section method to obtain  $\bar{E}$ .



We refer to [16, 40] for discussions related to the Dörlfer strategy for planewave approximations, in which no practical algorithm was implemented.

---

**Strategy B:** Error reduction

---

**Given:** eigenvalue tolerance  $\varepsilon > 0$ , energy cut-off  $E_c^{(k)}$  and error estimator  $\eta_{E_c^{(k)}}^{E_g}$ .

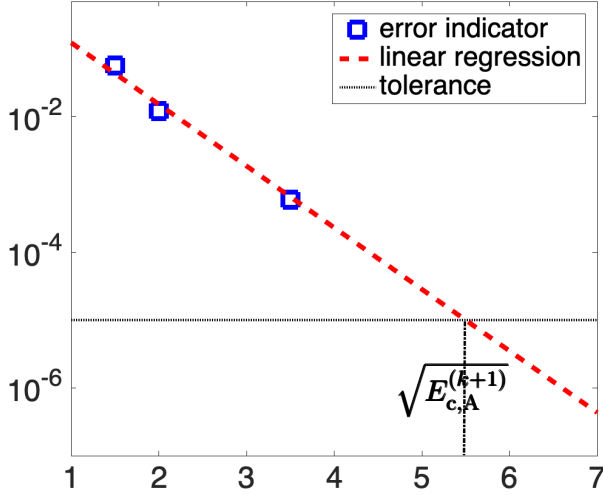
Find  $\bar{E} > E_c^{(k)}$  such that  $\bar{E}$  is the minimal value satisfying

$$\eta_{E_c^{(k)}}^{E_g}(\bar{E}) \geq \sqrt{\left(\eta_{E_c^{(k)}}^{E_g}\right)^2 - \varepsilon}. \quad (3.3)$$

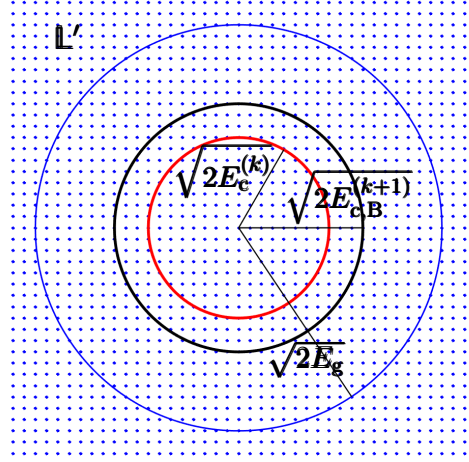
**Return:** Output energy cut-off  $E_{c,B}^{(k+1)} = \bar{E}$

---

From a practical point of view, it is more stable and reliable to use the combination of the above two strategies, which we describe in Algorithm 1 below.



(a) Strategy A.



(b) Strategy B.

Figure 3.1: Strategies for determining the energy cut-offs.

---

**Algorithm 1:** Adaptive planewave method for linear eigenvalue problems

---

**Given:** eigenvalue tolerance  $\varepsilon > 0$ , initial energy cut-off  $E_c^{(0)}$ ,  $E_g \gg 1$  and  $k = 0$ .

1. Solve (2.7) within  $X_{E_c^{(k)}}$  to obtain the planewave approximation  $(\lambda_{E_c^{(k)}}, \varphi_{E_c^{(k)}})$ .
2. Compute the *a posteriori* error estimator defined by (A.4) or (A.9).
3. If  $\left(\eta_{E_c^{(k)}}^{E_g}\right)^2 < \varepsilon$ , then stop and return the planewave approximation. Else, goto 4.
4. If  $k = 0$ , then use Strategy B to get  $E_c^{(k+1)} = E_{c,B}^{(k+1)}$ , let  $k = k + 1$  and goto 2.

Else, use Strategy A to compute  $E_{c,A}^{(k+1)}$  and Strategy B to compute  $E_{c,B}^{(k+1)}$ . Take

$$E_c^{(k+1)} = \min \left\{ E_{c,A}^{(k+1)}, E_{c,B}^{(k+1)} \right\} \quad (3.4)$$

and  $k = k + 1$ , goto 1.

**Return:**  $(\lambda_{E_c^{(k)}}, \varphi_{E_c^{(k)}})$

---

Note that we took ‘min’ in (3.4) in order to reduce the risk of overestimating the new energy cut-off. Alternatively, one can use ‘max’ in (3.4) instead of ‘min’ to minimize the number of iteration steps (and hence the number of calls to the linear eigensolver) in the algorithm. Since the computational cost for both error indicators and Strategy B increase with respect to the cut-off  $E_g$ , we can adjust  $E_g$  during the adaptive algorithms according to the energy cut-off  $E_c$ , to avoid using very large  $E_g$  throughout the algorithm.

Let us now comment on the computational cost of the algorithm, assuming that we need to compute  $m$  eigenvalues. At each step of Algorithm 1, the cost for solving the eigenvalue problem is  $\mathcal{O}(mE_c^d)$ , the cost for evaluating the error indicators is  $\mathcal{O}(mE_g^d)$  with (A.4), and  $\mathcal{O}(mE_g^{d/2})$  with the perturbation-method-based (A.9). Therefore, if a perturbation-method-based error indicator is used, or if  $E_g$  stays relatively small and comparable to  $E_c$  then the overall computational costs of Algorithm 1 is  $\mathcal{O}(m\bar{E}_c^d)$ , where  $\bar{E}_c$  is the optimal energy cut-off derived by the algorithm. Hence, the cost of the whole procedure is still dominated by the linear eigensolver. Compared to a classical convergence test, this procedure avoids the dependency on the user’s experience to find a good energy cut-off.

## 4 Applications to nonlinear eigenvalue problems

In this section, we will introduce an adaptive planewave method for nonlinear eigenvalue problems. We will first briefly review the Kohn–Sham equations, a widely used model in electronic structure calculations as well as its formulation in the framework of the projector augmented wave (PAW) method. We will then discuss how the adaptive algorithms developed for linear eigenvalue problems can be generalized to these nonlinear eigenvalue problems. We mention that only the error estimates for linear eigenvalue problems are required for the algorithms presented in this section.

## 4.1 Kohn–Sham equations

In the *ab-initio* quantum mechanical modeling of many electron systems, the Kohn–Sham density functional theory (DFT) [31, 33] has established itself as one of the most powerful electronic structure methods due to its good balance between accuracy and computational cost.

We consider a many-particle system (with  $N_{\text{atom}}$  nuclei and  $N_e$  electrons) in the spinless and non-relativistic setting. The Kohn–Sham ground state solution can be obtained by solving the following Kohn–Sham equations [37]: Find  $(\lambda_i, \varphi_i) \in \mathbb{R} \times H_{\#}^1(\Omega)$ ,  $i = 1, \dots, N_b$ , such that  $\int_{\Omega} \varphi_i \varphi_j = \delta_{ij}$  and

$$H[\rho]\varphi_i = \lambda_i \varphi_i, \quad (4.1)$$

where  $N_b$  is the number of eigenpairs/bands under consideration,  $\{\lambda_i\}_{i=1}^{N_b}$  are the  $N_b$  lowest eigenvalues,  $\rho = \sum_{i=1}^{N_b} f_i |\varphi_i|^2$  is the electron density with  $f_i$  the occupancy number, and

$$H[\rho] = -\frac{1}{2}\Delta + V_{\text{eff}}[\rho] \quad \text{and} \quad V_{\text{eff}}[\rho] = v_{\text{ps}} + v_{\text{H}}[\rho] + v_{\text{xc}}[\rho] \quad (4.2)$$

with  $V_{\text{eff}}[\rho]$  the effective potential,  $v_{\text{ps}}$  the pseudo-potential generated by the nuclei and core electrons,  $v_{\text{H}}[\rho]$  and  $v_{\text{xc}}[\rho]$  the so-called Hartree potential and exchange-correlation potential, respectively. The occupancy numbers  $f_i$  can be chosen by smearing methods like the Fermi–Dirac or the Methfessel–Paxton scheme.

We shall now give more details on the potentials used to define  $V_{\text{eff}}$ . In the norm-conserving pseudo-potential setting [37], the pseudo-potential  $v_{\text{ps}}$  can be written as

$$v_{\text{ps}} = v_{\text{loc}} + v_{\text{nl}},$$

where  $v_{\text{loc}} : \mathbb{R}^d \rightarrow \mathbb{R}$  is the local part,  $v_{\text{nl}}$  is a non-local operator given by

$$(v_{\text{nl}}\phi)(\mathbf{r}) = \sum_{I=1}^{N_{\text{atom}}} \sum_{j=1}^{M_{\text{ps}}} (\phi, \xi_{I,j}) \xi_{I,j}(\mathbf{r}) \quad \forall \phi \in L_{\#}^2(\Omega) \quad (4.3)$$

with  $M_{\text{ps}} \in \mathbb{Z}_+$  and  $\xi_{I,j}$  ( $I = 1, \dots, N_{\text{atom}}$ ,  $j = 1, \dots, M_{\text{ps}}$ )  $\in L_{\#}^2(\Omega)$  being sufficiently smooth functions in  $\mathbb{R}^d$ . In the context of ultra-soft pseudo-potentials (USPP) or PAW methods [36, 49], the non-local parts are formulated by

$$(v_{\text{nl}}\varphi)(\mathbf{r}) = \sum_{I=1}^{N_{\text{atom}}} \sum_{n,m=1}^{M_{\text{ps}}} D_{nm}^I(\beta_{I,m}, \varphi) \beta_{I,n}(\mathbf{r}) \quad \forall \varphi \in L_{\#}^2(\Omega), \quad (4.4)$$

where  $D_{nm}^I$  depends on eigenfunctions and need to be updated during the SCF loop. For more details on the PAW method, which will be the model we use in practice for the numerical experiments in Section 5, see Appendix B.

In periodic systems,  $v_{\text{H}}[\rho]$  represents the  $\mathbb{L}$ -periodic Coulomb potential generated by the  $\mathbb{L}$ -periodic electron density  $\rho$

$$v_{\text{H}}[\rho](\mathbf{r}) = 4\pi \sum_{\mathbf{G} \in \mathbb{L}' \setminus \{0\}} |\mathbf{G}|^{-2} \hat{\rho}_{\mathbf{G}} e_{\mathbf{G}}(\mathbf{r}).$$

Finally, for the exchange-correlation potential, we use a generalized gradient approximation (GGA) [42] in our numerical experiments.

Problem (4.1) is a nonlinear eigenvalue problem since the operator depends on the electron density  $\rho$ , and hence the eigenfunctions  $\{\varphi_i\}_{i=1}^{N_b}$ . A self-consistent field (SCF) iteration algorithm [37] is commonly resorted to for this kind of nonlinear eigenvalue problem. At each iteration, a new Hamiltonian is constructed from a trial electronic state and a linear eigenvalue problem, in the form of Schrödinger-type equation (2.1), is then solved to obtain the low-lying eigenvalues and corresponding eigenvectors.

In the first iterations of the self-consistent field algorithm, the iterates are far from the exact solution, so that the error coming from the iterative solver is dominant. But close to self-consistency, the choice of the basis set becomes important, as the basis set size will ultimately determine the quality of the final approximation. Therefore, an efficient planewave SCF algorithm should be able to adjust the energy cut-off on the fly, so that no computational resource is wasted while the required accuracy can be reached at the end of the iterations. We refer to [24] for a similar discussion of error balancing for Gross-Pitaevskii equations.

## 4.2 Adaptive algorithm for nonlinear problems

We now discuss the construction of error indicators and the adaptive algorithm for the nonlinear Kohn–Sham equations (4.1). As mentioned in Section 4.1, an SCF iteration algorithm is used to solve the nonlinear eigenvalue problems, in which a linear Schrödinger-type equation is solved at each step. Therefore, we can incorporate Algorithm 1 (for linear problems) into each SCF iteration, and thus adapt the energy cut-off on the fly with some well-chosen tolerance, corresponding to the self-consistency error. The use of the self-consistency error as the tolerance for adapting the cut-off is based on the following: when the solution is far from self-consistency, one can choose a relative small energy cut-off for the linearized eigenvalue problem; when the iteration is close to self-consistency, one has to use a large energy cut-off to obtain accurate eigenpairs.

Let  $\rho_{\text{in}}^{(m)}$  and  $\rho_{\text{out}}^{(m)}$  represent the input and output electron densities at the  $m$ -th step of the SCF algorithm. At the  $m$ -th step, a linearized eigenvalue problem, with the trial input electron density  $\rho_{\text{in}}^{(m)}$  is solved

$$H[\rho_{\text{in}}^{(m)}]\varphi_i^{(m)} = \lambda_i^{(m)}\varphi_i^{(m)} \quad i = 1, 2, \dots, N_b \quad (4.5)$$

with some energy cut-off  $E_c^{(m)}$ . Then an output electron density  $\rho_{\text{out}}^{(m)}$  is obtained from the eigenfunctions  $\{\varphi_i^{(m)}\}_{i=1}^{N_b}$ . The self-consistency error is defined by

$$\eta_{\text{SCF}}^{(m)} := \alpha^{1/2} \|\rho_{\text{in}}^{(m)} - \rho_{\text{out}}^{(m)}\|_{L^2(\Omega)} \quad \text{for some } \alpha > 0. \quad (4.6)$$

The parameter  $\alpha$  in (4.6) is tuning the ratio of self-consistency error to discretization error in the total error. In Section 5, we test different  $\alpha$ 's numerically. Note that  $\alpha$  could be chosen based on the *a posteriori* error estimates for the nonlinear problem, which will be investigated in future work.

The planewave discretization error indicator is defined with respect to the linear eigenvalue problem (4.5), which involves all  $N_b$  eigenpairs under consideration, as discussed in Remark 2.2. In analogy with definition (2.13), we define the discretization error indicator as

$$\eta_{E_c}^{(m)} := \left( \sum_{i=1}^{N_b} f_i \|\text{Res}_i^{(m)}\|_{a'}^2 \right)^{1/2} \quad (4.7)$$

where  $f_i$  is the occupancy number,  $\|\cdot\|_{a'}$  is the dual norm corresponding to the linear operator

$$A^{(m)} := H[\rho_{\text{in}}^{(m)}],$$

and  $\text{Res}_i^{(m)}$  is the residual for the  $i$ -th eigenpair at the  $m$ -th step

$$\text{Res}_i^{(m)} := H[\rho_{\text{in}}^{(m)}]\varphi_i^{(m)} - \lambda_i^{(m)}\varphi_i^{(m)} \in H'. \quad (4.8)$$

With a given  $E_g \gg E_c^{(m)}$ , we define the computable discretization error indicator by

$$\eta_{E_c}^{E_g, (m)} := \sum_{i=1}^{N_b} f_i \left( \sum_{\mathbf{G} \in \mathbb{L}', E_c \leq \frac{1}{2}|\mathbf{G}|^2 \leq E_g} \widehat{\text{Res}_i^{(m)} \mathbf{G}}^{E_g} \cdot \widehat{A^{(m), -1} \text{Res}_i^{(m)} \mathbf{G}}^{E_g} \right)^{\frac{1}{2}} \quad (4.9)$$

based on the standard calculation (A.4), and

$$\eta_{E_c}^{E_g, (m), [k]} := \sum_{i=1}^{N_b} f_i \left( \sum_{\mathbf{G} \in \mathbb{L}', E_c \leq \frac{1}{2}|\mathbf{G}|^2 \leq E_g} \widehat{\text{Res}_i^{(m)} \mathbf{G}}^{E_g} \cdot \widehat{A^{(m), -1, [k]} \text{Res}_i^{(m)} \mathbf{G}}^{E_g} \right)^{\frac{1}{2}} \quad \text{with } k = 1, 2 \quad (4.10)$$

based on a perturbation method (A.9).

Combining the SCF algorithm and Algorithm 1 for linear eigenvalue problems, we propose the following adaptive algorithm for nonlinear eigenvalue problems.

---

**Algorithm 2:** Adaptive planewave method for nonlinear eigenvalue problems

---

**Given:** tolerance  $\delta > 0$ , initial energy cut-off  $E_c^{(1)}$ ,  $E_g \gg 1$ ,  $m = 1$  and  $\rho^{(0)} \in L_{\#}^2(\Omega)$

1. Solve (4.5) with the trial electron density  $\rho^{(m-1)}$  within  $X_{E_c^{(m)}}$  to obtain the plane wave approximations  $\left\{ (\lambda_{j, E_c^{(m)}}^{(m)}, \varphi_{j, E_c^{(m)}}^{(m)}) \right\}_{j=1}^{N_b}$ . Compute the error indicator  $\eta_{\text{SCF}}^{(m)}$ .
2. Compute the error indicator  $\eta_{E_c^{(m)}}^{E_g, (m)}$  (or  $\eta_{E_c^{(m)}}^{E_g, (m), [k]}$ ).
3. If  $\left( \eta_{\text{SCF}}^{(m)} \right)^2 < \delta$  and  $\left( \eta_{E_c^{(m)}}^{E_g, (m)} \right)^2 < \delta$ , then stop and return the approximations. Else, goto 4.
4. If  $\left( \eta_{E_c^{(m)}}^{E_g, (m)} \right)^2 < \left( \eta_{\text{SCF}}^{(m)} \right)^2$ , then goto 5.

Else, use Algorithm 1 to solve (4.5) with tolerance  $\varepsilon = \left( \eta_{\text{SCF}}^{(m)} \right)^2$ , let  $E_c^{(m)}$  be the final energy cut-off of Algorithm 1, goto 5.

5. Let  $\rho^{(m)}$  be the electron density from  $\left\{ \varphi_{j, E_c^{(m)}}^{(m)} \right\}_{i=1}^{N_b}$  and  $m = m + 1$ , goto 1.

**Return:** Approximate eigenfunctions and eigenvalues  $\left\{ (\lambda_{j, E_c^{(m)}}^{(m)}, \varphi_{j, E_c^{(m)}}^{(m)}) \right\}_{j=1}^{N_b}$

---

In Step 4 of Algorithm 2, by taking  $\left(\eta_{\text{SCF}}^{(m)}\right)^2$  as the tolerance for plane wave discretizations, we are actually estimating the total energy error of the full nonlinear eigenvalue problem by the sum  $\left(\eta_{E_c}^{(m)}\right)^2 + \left(\eta_{\text{SCF}}^{(m)}\right)^2$ . We note that it could be possible to construct some *a posteriori* error estimate for the nonlinear eigenvalue problems directly (see [10, 18, 20, 24]). However, we will not use or discuss this type of estimates in this work.

In Step 5 of Algorithm 2, one can exploit a charge mixing scheme to ensure or accelerate the convergence of the SCF algorithm.

The most important feature of Algorithm 2 is that it is adaptive. It automatically determines a good discretization parameter, in our case the energy cut-off, on the fly to achieve the required accuracy. Moreover, compared to the conventional SCF iteration, Algorithm 2 avoids solving large linear eigenvalue problems at all iteration steps. Since the energy cut-offs are determined on the fly and increase during the SCF iterations, a lot of computational cost can be saved from that one only needs to solve small eigenvalue problems while the solution is still away from convergence. The extra cost of this adaptive algorithm comes from calculating the error indicator. Note that the cost for each eigenpair is  $\mathcal{O}(E_g^d)$ , and hence the total cost for  $N_b$  eigenpairs is  $\mathcal{O}(N_b E_g^d)$ . For perturbation-based error indicator, the cost is reduced to  $\mathcal{O}(N_b E_g^{d/2})$ . Since the cost for one linear eigensolver is  $\mathcal{O}(N_b E_c^d)$  and  $E_g$  is proportional to  $E_c$ , we have that the additional cost for calculating the error indicator is way smaller than the cost saved from the linear eigensolvers used with small energy cut-offs.

## 5 Numerical experiments

In this section, we will first test our adaptive algorithms on simple linear and nonlinear eigenvalue problems, and then show the performance on solving the electronic structure of typical bulk systems with the PAW method. The approximation errors are calculated with respect to the reference solutions obtained with a sufficiently large energy cut-off.

### 5.1 Tests of principle

**A linear eigenvalue problem.** Consider the 2D linear eigenvalue problems of the form (2.1), with  $\Omega = [-5, 5]^2$  and  $V(x, y) = 1.5(x^2 + y^2) + e^{-(x-1)^2 - y^2}$ . We use a large energy cut-off  $E_c = 100.0$  to obtain the “exact” solution in this example.

We first compare in Figure 5.1 the numerical errors in the lowest two eigenvalues with the different *a posteriori* error indicators discussed in Section 2.4 and Appendix A. We observe in the plots that they match almost perfectly. Moreover, the errors decay exponentially with respect to the energy cut-off which suggests that a linear regression strategy could work well. We also observe that in this case, the first order perturbation method ((A.9) with  $k = 1$ ) to compute the error indicator already leads to a very accurate approximation of the true error.

We further test the adaptive algorithm (Algorithm 1) on this linear problem. Tables 1 and 2 show the energy cut-offs obtained by using the error indicators (A.5) and (A.9) respectively, with Strategy A and Strategy B, and tolerances  $\varepsilon = 10^{-3}$  and  $10^{-6}$ . We obtain by performing a traditional convergence test that the optimal cut-offs for these two tolerances are 7.1 and 16.0 respectively. Algorithm 1 captures energy cut-offs respectively of 7.5 and 17.12 in a few steps, which suffice for the target accuracy without overshooting too much the optimal cut-offs.

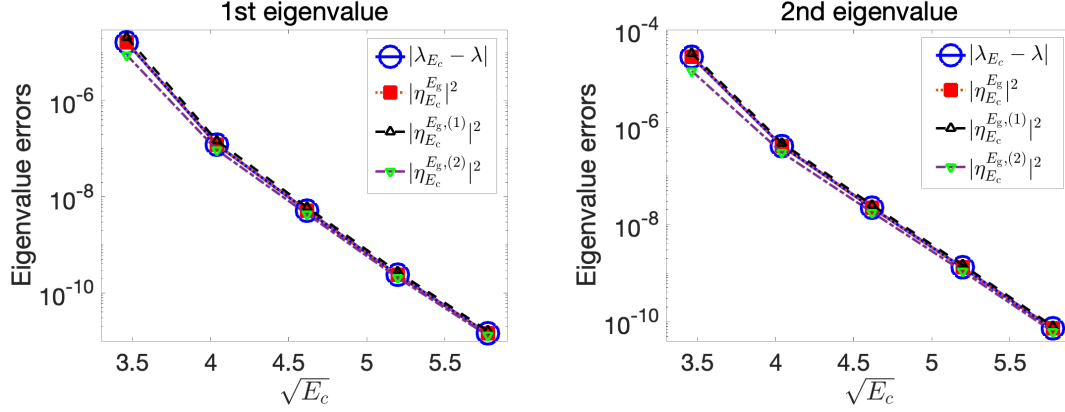


Figure 5.1: Linear problem: Numerical errors of the 1st and 2nd eigenvalues and the *a posteriori* error estimators. The quantity  $|\eta_{E_c}^{E_g}|^2$  is defined in (A.5) and  $|\eta_{E_c}^{E_g, (1)}|^2$  and  $|\eta_{E_c}^{E_g, (2)}|^2$  are defined in (A.9).

Table 1: Linear problem: Error indicators and energy cut-offs obtained by Algorithm 1 with (A.5).

tolerance $\varepsilon = 1.0\text{e-}3$					tolerance $\varepsilon = 1.0\text{e-}6$				
step	$E_c$	$\eta_{E_c}^2$	$E_{c,A}$	$E_{c,B}$	step	$E_c$	$\eta_{E_c}^2$	$E_{c,A}$	$E_{c,B}$
0	3.00	5.121543e-01	—	7.50	0	3.00	5.121543e-01	—	12.00
1	7.50	5.370600e-04	—	—	1	12.00	5.329866e-05	17.12	21.00
					2	17.12	4.715432e-07	—	—

Table 2: Linear problem: Error indicators and energy cut-offs obtained by Algorithm 1 with (A.9),  $k = 1$ .

tolerance $\varepsilon = 1.0\text{e-}3$					tolerance $\varepsilon = 1.0\text{e-}6$				
step	$E_c$	$\eta_{E_c}^2$	$E_{c,A}$	$E_{c,B}$	step	$E_c$	$\eta_{E_c}^2$	$E_{c,A}$	$E_{c,B}$
0	3.00	3.807044e-01	—	7.50	0	3.00	3.807044e-01	—	12.00
1	7.50	2.898487e-04	—	—	1	12.00	3.339172e-05	16.93	21.00
					2	16.93	3.395260e-07	—	—

**A nonlinear eigenvalue problem.** Consider the following Gross-Pitaevskii equation (GPE) originated from modelling Bose-Einstein condensates [43]: Find  $(\lambda, \varphi) \in \mathbb{R} \times H_{\#}^1(\Omega)$ , such that  $\|\varphi\|_{L^2(\Omega)} = 1$  and

$$\left(-\frac{1}{2}\Delta + V(\mathbf{r}) + \mu\rho(\mathbf{r})\right)\varphi(\mathbf{r}) = \lambda\varphi(\mathbf{r}) \quad (5.1)$$

where  $\mu = 1.0$ ,  $\Omega = [-5, 5]^2$ ,  $V(x, y) = 10(x^2 + y^2) + e^{-((x-1)^2 + y^2)}$ , and  $\rho(\mathbf{r}) = |\varphi(\mathbf{r})|^2$ .

Note that this equation can be viewed as a simplified version of (4.1), where only the lowest eigenvalue is considered and the nonlinear term is much simpler.

We apply Algorithm 2 to solve (5.1) with tolerance  $\delta = 10^{-6}$ , and  $\alpha = 1.0$  and  $0.1$  ( $\alpha$  is the parameter in (4.7)), respectively. We show in Figure 5.2 the discretization and SCF errors with respect to the SCF steps. The energy cut-off is iteratively adjusted with Algorithm 2 and we observe that a good balance is achieved between the SCF and discretization errors. The oscillation in the SCF errors arises from the simple mixing scheme used in the SCF iterations.

As a comparison, we perform plain SCF calculations, without adapting the energy cut-off, by taking the fixed “optimal” energy cut-off  $E_c = 17.4$ , obtained from a careful convergence test. It takes respectively 12 and 10 SCF steps to achieve self-consistency  $\|\rho_{\text{in}} - \rho_{\text{out}}\|_{L^2(\Omega)}^2 < \epsilon$  with tolerance  $\epsilon = 10^{-6}$  and  $10^{-5}$  respectively. These two cases are compared with Algorithm 2 with  $\alpha = 1.0$  and  $0.1$  (the two plots in Figure 5.2) cases, which call the linear eigensolver 23 and 12 times, respectively. Note that we compare the  $\alpha = 0.1$  case with the plain SCF iterations with tolerance  $10^{-5}$  since they give the same criterion for self-consistency. We see that the number of calls to the linear solver in the adaptive algorithm with  $\alpha = 0.1$  is similar to the non adaptive case, while our adaptive algorithm uses much smaller energy cut-offs at the early iterations.

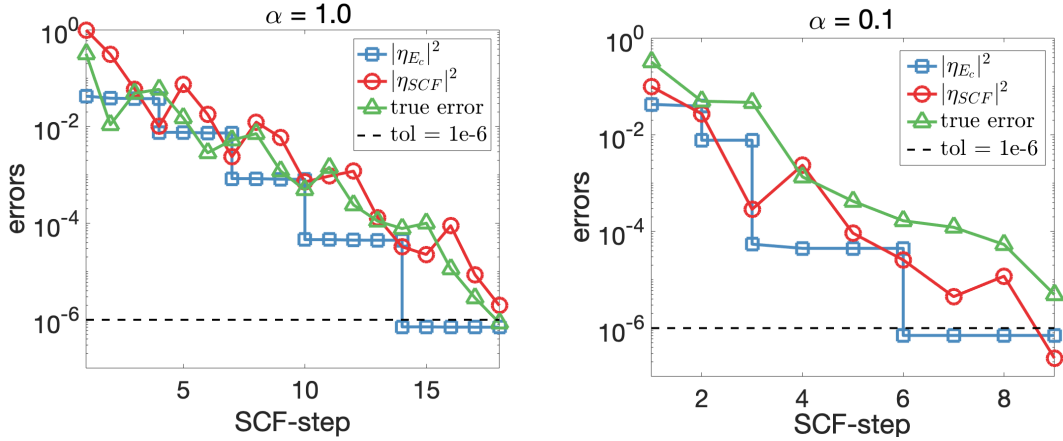


Figure 5.2: Nonlinear problem: Discretization, SCF and true eigenvalue errors obtained by Algorithm 2.

## 5.2 Tests on PAW Kohn–Sham equations

We implemented the *a posteriori* error indicator and the adaptive algorithm (Algorithm 2) in an in-house planewave PAW code [27]. For the tests of validity we chose two bulk systems. The first is a diamond structure with two carbon atoms in the unit cell. This is an insulator and we used only the  $\Gamma$  point for the  $k$ -sampling. The number of occupied bands is  $N_b = 4$ . The second system is an FCC structure with four aluminum atoms in the unit cell. It is a metallic system with a vanishing band gap, and we employed a  $6 \times 6 \times 6$  Monkhorst–Pack  $k$ -mesh. The first order Methfessel–Paxton smearing method [38] with a smearing width of  $0.3 \text{ eV}$  was used and the number of occupied bands is  $N_b = 7$ . For the tests of efficiency, we constructed a  $4 \times 4 \times 4$  diamond supercell containing 128 carbon atoms, and the number of occupied bands is  $N_b = 256$ .



Table 3: Comparison of estimated errors and real error in  $E_{\text{bands}}$  for the linearized Kohn–Sham equation of the diamond structure. The  $E_c$  and error data are in eV. The relative differences are calculated w.r.t. the real error. The reference solution is obtained with  $E_c = 4500$  eV.

$E_c$	Real error	$ \eta_{E_c}^{E_g,[1]} ^2$		$ \eta_{E_c}^{E_g,[2]} ^2$		$ \eta_{E_c}^{E_g} ^2$	
400.0	2.445e-01	2.190e-01	-10.44 %	2.336e-01	-4.46 %	2.385e-01	-2.45 %
600.0	2.329e-02	2.163e-02	-7.11 %	2.256e-02	-3.11 %	2.264e-02	-2.78 %
800.0	9.093e-03	8.684e-03	-4.50 %	8.889e-03	-2.25 %	8.891e-03	-2.23 %
1000.0	2.690e-03	2.574e-03	-4.29 %	2.630e-03	-2.21 %	2.632e-03	-2.15 %
1200.0	1.684e-03	1.631e-03	-3.18 %	1.657e-03	-1.65 %	1.655e-03	-1.73 %
1400.0	7.283e-04	7.133e-04	-2.07 %	7.230e-04	-0.73 %	7.251e-04	-0.45 %

Table 4: Comparison of estimated errors and real error in  $E_{\text{bands}}$  for the linearized Kohn–Sham equation of the FCC aluminum system. Energy unit and relative difference calculation are the same as in Table 3. The reference solution is obtained with  $E_c = 2000$  eV.

$E_c$	Real error	$ \eta_{E_c}^{E_g,[1]} ^2$		$ \eta_{E_c}^{E_g,[2]} ^2$		$ \eta_{E_c}^{E_g} ^2$	
300.0	2.035e-02	1.805e-02	-11.29 %	1.936e-02	-4.87 %	2.000e-02	-1.71 %
400.0	4.484e-03	4.248e-03	-5.27 %	4.404e-03	-1.78 %	4.445e-03	-0.88 %
500.0	1.810e-03	1.733e-03	-4.25 %	1.790e-03	-1.10 %	1.799e-03	-0.64 %
600.0	9.420e-04	9.046e-04	-3.97 %	9.333e-04	-0.92 %	9.368e-04	-0.55 %
700.0	5.262e-04	5.032e-04	-4.37 %	5.219e-04	-0.82 %	5.240e-04	-0.42 %
800.0	3.249e-04	3.120e-04	-3.96 %	3.225e-04	-0.75 %	3.237e-04	-0.37 %

In the following, we first check the accuracy of the *a posteriori* error indicators on the linearised Kohn–Sham equations and then test the behavior of the adaptive algorithm for solving the nonlinear equations. In order to take into account all the  $N_b$  occupied eigenstates, we present error results of the so-called band structure energy  $E_{\text{bands}} \equiv \sum_{n=1}^{N_b} f_n \epsilon_n$  where  $f_n$  denotes the occupation number of the  $n$ th eigenstate and  $\epsilon_n$  is the eigenvalue.

**Accuracy of the error indicators for the linearized Kohn–Sham equations.** We are primarily concerned with the accuracy of the error indicator for the linearized Kohn–Sham equation since it determines the effectiveness of the adaptive algorithm. In our tests we fixed the density as the superposition of atomic charge densities and solved the linearized Kohn–Sham equations under different energy cut-off values  $E_c$ . The *a posteriori* error indicators were calculated by using the standard and the perturbation-based methods detailed in Appendix A.

The error indicators  $|\eta_{E_c}^{E_g}|^2$ ,  $|\eta_{E_c}^{E_g,[1]}|^2$ , and  $|\eta_{E_c}^{E_g,[2]}|^2$  are compared with real errors in Table 3 and Table 4 for the diamond structure and the aluminum systems, respectively. We see that errors estimated by the standard indicator  $|\eta_{E_c}^{E_g}|^2$  closely match the real error for all  $E_c$  values. Moreover, the second-order indicator  $|\eta_{E_c}^{E_g,[2]}|^2$  exhibits a clear improvement over the first-order indicator  $|\eta_{E_c}^{E_g,[1]}|^2$  and derives error results that are very close to those from the standard indicator.

In terms of cost, however, the standard indicator is remarkably more expensive than the perturbation-based indicators, as illustrated by time statistics for the diamond example in Table 5. The standard indicator requires to solve a linear system of size  $N_{E_g}$  for each of

Table 5: The CPU time cost (in seconds) of the standard and perturbation-based error indicators for the diamond structure. The numbers of degrees of freedom in the eigenvalue computation ( $N_{E_c}$ ) and error estimation grids ( $N_{E_g}$ ) are also provided.

$E_c$	$N_{E_c}$	$N_{E_g}$	1st-order	2nd-order	Standard
400.0	91	534	0.01	0.02	0.62
600.0	170	995	0.02	0.05	1.22
800.0	281	1536	0.03	0.06	1.86
1000.0	435	2140	0.06	0.11	3.33
1200.0	534	2801	0.08	0.15	4.72
1400.0	682	3488	0.10	0.17	5.87

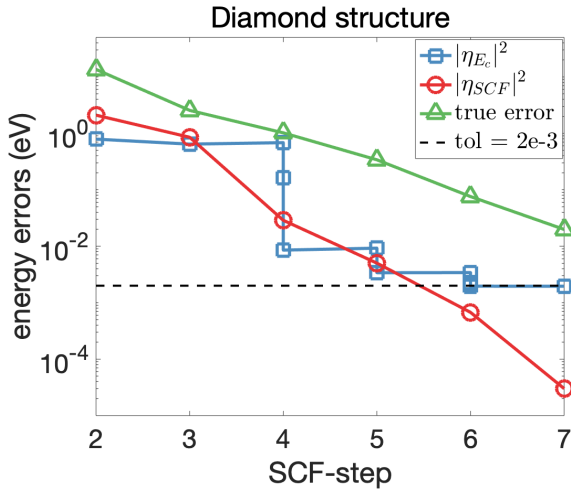


Figure 5.3: Diamond structure: Discretization and SCF errors in the adaptive solutions to the Kohn–Sham equations using Algorithm 2.

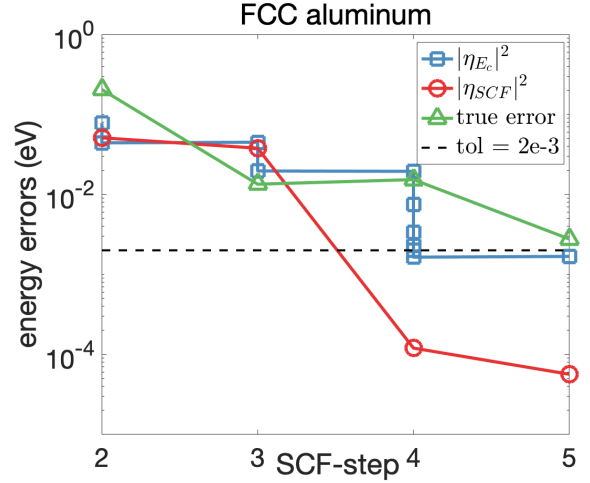


Figure 5.4: FCC aluminum: Discretization and SCF errors in the adaptive solution to the Kohn–Sham equations using Algorithm 2.

the  $N_b$  eigenvalues, the time complexity of which is  $\mathcal{O}(N_b N_{E_g} \log(N_{E_g}))$  using the planewave method. Noting that the complexity for solving the eigenvalue problem is  $\mathcal{O}(N_b^2 N_{E_c})$  and  $N_{E_g}$  is several times larger than  $N_{E_c}$ , we see that in the case of small systems, time costs of the standard indicator may be of same order or even larger than solving the eigenvalue problem.

Therefore, the perturbation-based calculation of the *a posteriori* error estimate is the proper choice in practice to balance accuracy versus computational cost. We employed the first-order indicator in the following tests. It should be emphasized that the proposed error estimate is accurate both for the tested insulator and metallic systems. This high-quality *a posteriori* error indicator is critical to a reliable tuning of the energy cut-off.

**Adaptive solution of the Kohn–Sham equation with an unknown converged cut-off.** We now apply Algorithm 2 to solve the nonlinear Kohn–Sham equations. The density mixing is performed using Pulay’s DIIS method [44]. The tolerance for the discretization error in  $E_{\text{bands}}$  and that for the SCF error were chosen to be  $2 \times 10^{-3}$  eV for both the diamond structure and the aluminum systems.

The evolution of the discretization and SCF errors with respect to the SCF step are shown

Table 6: Diamond structure: Detailed  $E_c$  and error data during the adaptive solution of the Kohn–Sham equations by Algorithm 2. The  $E_c$  and errors are in eV.

SCF-step	$E_c$	$ \eta_{E_c} ^2$	$ \eta_{\text{SCF}} ^2$
2	300	7.895e-01	2.099
3	300	6.439e-01	8.518e-01
4	300	6.837e-01	2.878e-02
	400	1.622e-01	
	794.42	8.537e-03	
5	794.42	9.242e-03	5.018e-03
	894.42	3.393e-03	
6	894.42	3.414e-03	6.735e-04
	994.42	2.260e-03	
	1044.42	2.100e-03	
	1094.42	1.960e-03	
7	1094.42	1.956e-03	3.004e-05

in Figure 5.3 and Figure 5.4 for the diamond and the aluminum systems, respectively. For a detailed illustration, we take the diamond structure and further present detailed data on the energy cut-off and the two components of errors in Table 6. It is seen that a converged solution is obtained by adaptively tuning the energy cut-off depending on the discretization and SCF errors.

**Comparison of time costs with convergence-test computations.** We have stated in the introduction section that the purpose of our adaptive algorithm is to determine the converged energy cut-off in an *a posteriori* way and avoid the usual convergence-test computations. In this part we compare the computational cost of the adaptive algorithm with convergence-test computations quantitatively. Noting that the execution time for solving the above primitive-cell systems is too short, in order to make a meaningful time comparison we carried out tests here on a larger system, i.e. a  $4 \times 4 \times 4$  diamond supercell which contains 128 carbon atoms.

The tolerance for the discretization error in  $E_{\text{bands}}$  and that for the SCF error were set as 0.15 eV (about 0.001 eV/atom). In the adaptive solution, we started with an energy cut-off of  $E_c = 300$  eV and adaptively tuned the cut-off until the convergence of  $E_{\text{bands}}$ . In the convergence-test computations, we began with  $E_c = 300$  eV and gradually increased the cut-off with a step of 100 eV. The Kohn–Sham equations were solved under the increasing cut-off values until the difference in  $E_{\text{bands}}$  between successive calculations is smaller than the tolerance.

We present time cost of the adaptive algorithm and that of the convergence-test computations in Table 7 and Table 8, respectively. The time cost of the adaptive algorithm is composed of two parts denoted by  $t_{\text{eigen}}$  for solving the eigenvalue problems and  $t_{\text{err}}$  for calculating the *a posteriori* error estimate. It is seen from Table 7 that  $t_{\text{eigen}}$  and  $t_{\text{err}}$  for the adaptive solution of the diamond supercell are 156.32 s and 27.16 s in total, respectively. In the convergence-test computations, however, time cost of the solution of Kohn–Sham equations accumulated to 734.44 s, as shown in Table 8. Compared with the convergence-test

Table 7: Time cost (in seconds) of the adaptive algorithm for solving the Kohn–Sham equation of the diamond supercell where  $t_{\text{eigen}}$  represents the time for solving the eigenvalue problem and  $t_{\text{err}}$  the time for calculating the *a posteriori* error estimate. The reason for the discontinuous SCF step index in the following is that, when the discretization error is detected to be smaller than the SCF error, we take the discretization error as the tolerance and perform more than one SCF iteration until convergence.

SCF-step	$E_c$	$t_{\text{eigen}}$	$t_{\text{err}}$
2	300	14.33	1.04
6	300	9.76	1.04
	400	9.65	1.46
	538.83	12.78	2.57
	805.86	14.59	2.71
10	805.86	39.91	5.28
	905.86	18.48	5.83
	1004.61	22.89	7.23
12	1004.61	13.93	–
Total		156.32	27.16

Table 8: Time cost (in seconds) of the convergence-test computations for the Kohn–Sham equation of the diamond supercell.

$E_c$	300	400	500	600	700	800	900	1000	
$t_{\text{eigen}}$	27.21	43.10	62.12	75.11	97.54	111.58	142.25	175.53	Total=734.44

computations, the adaptive algorithm leads to a remarkable saving in the computation time.

## 6 Conclusions and perspectives

In this paper, we constructed an adaptive planewave method for linear eigenvalue problems and further integrated it into a self-consistent field algorithm for nonlinear eigenvalue problems. The algorithm combines the knowledge of *a priori* error decay and the construction of *a posteriori* error indicators that is asymptotically accurate and computable. This adaptive method not only provides good energy cut-offs in planewave methods for linear eigenvalue problems, but also shows potential for the adaptive resolution of Kohn-Sham equations in electronic structure calculations.

For now, we have only considered the error from the planewave discretizations. In real calculations though, in particular to compute physical quantities, other sources of errors come into play, such as the integration over the Brillouin zone (after Bloch's decomposition [37]). Standard methods rely on equally spaced grid points and there is no reliable *a posteriori* error estimate for this error. This will need to be further investigated, in order to develop efficient numerical methods for periodic systems that can estimate, control and balance the errors from planewave discretizations, SCF iterations, and Brillouin zone integrations.

## Acknowledgement

B. Liu and H. Chen's work was supported by the National Natural Science Foundation of China under grant 11971066. G. Dusson's work was partially supported by the French "Investissements d'Avenir" program, project ISITE-BFC (contract ANR-15-IDEX-0003). J. Fang's work was supported by the National Natural Science Foundation of China under grant 11701037. X. Gao's work was supported by the Science Challenge Project under Grant TZ2018002.

# Appendices

## Appendix A Evaluating the *a posteriori* error indicator

In this section, we discuss how to evaluate (or approximate) the dual norm of the residual (in (2.13)) in an accurate and efficient way within the framework of planewave discretization. We present first a standard calculation and then a perturbation-based-method.

### A.1 A standard calculation

Let  $A = -\Delta + V$  be the linear operator with periodic boundary condition given in (2.1). From (2.3) we have that  $A$  is positive definite up to shifting by a positive constant, and hence  $A^{1/2}$  is well defined. From definition (2.13), we can obtain from a standard calculation and

Cauchy-Schwarz inequality that

$$\begin{aligned}\eta_{E_c} &= \sup_{v \in H} \frac{\langle \text{Res}_{E_c}, v \rangle_{H', H}}{\|v\|_a} = \sup_{v \in H} \frac{(A^{-1/2} \text{Res}_{E_c}, A^{1/2} v)}{\sqrt{(A^{1/2} v, A^{1/2} v)}} = \|A^{-1/2} \text{Res}_{E_c}\|_{L^2(\Omega)} \\ &= \langle \text{Res}_{E_c}, A^{-1} \text{Res}_{E_c} \rangle_{H', H}^{\frac{1}{2}} = \left( \sum_{\mathbf{G} \in \mathbb{L}'} \widehat{\text{Res}_{E_c} \mathbf{G}} \cdot A^{-1} \widehat{\text{Res}_{E_c} \mathbf{G}} \right)^{\frac{1}{2}}, \quad (\text{A.1})\end{aligned}$$

where  $\widehat{\text{Res}_{E_c}}$  and  $A^{-1} \widehat{\text{Res}_{E_c}}$  are the vectors of Fourier coefficients of  $\text{Res}_{E_c} \in H'$  and  $A^{-1} \text{Res}_{E_c} \in H$  respectively. For  $\mathbf{G} \in \mathbb{L}'$ ,

$$\widehat{\text{Res}_{E_c} \mathbf{G}} = \langle \text{Res}_{E_c}, e_{\mathbf{G}} \rangle_{H', H} \quad \text{and} \quad A^{-1} \widehat{\text{Res}_{E_c} \mathbf{G}} = (A^{-1} \text{Res}_{E_c}, e_{\mathbf{G}}).$$

To compute (A.1), we shall approximate  $L^2_{\#}(\Omega)$  by a finite dimensional subspace  $X_{E_g}(\Omega)$  (see definition (2.4)) with some  $E_g \gg E_c$ , that is, approximate the sum over  $\mathbf{G} \in \mathbb{L}'$  by finitely many terms  $\frac{1}{2}|\mathbf{G}|^2 \leq E_g$ . We refer to [8, Eq. (80)-(82)] and [9, Theorem 3.1] for an analysis of the numerical integration error from the cut-off  $E_g$ . In our practical simulations, we observe that when we choose  $E_g \geq 4E_c$ , then the integration error due to the cut-off  $E_g$  is negligible compared with the discretization error with cut-off  $E_c$ .

Using the orthogonality of the planewave basis functions and the fact that  $(\lambda_{E_c}, \varphi_{E_c})$  satisfies (2.7), the Fourier coefficients of the residual can be easily computed by

$$\widehat{\text{Res}_{E_c} \mathbf{G}} = a(\varphi_{E_c}, e_{\mathbf{G}}) - \lambda_{E_c}(\varphi_{E_c}, e_{\mathbf{G}}) = (V\varphi_{E_c} - \Pi_{E_c}(V\varphi_{E_c}), e_{\mathbf{G}}) \quad \forall \mathbf{G} \in \mathbb{L}'.$$

More precisely,  $\widehat{\text{Res}_{E_c}}$  can be approximated within  $X_{E_g}$  by

$$\widehat{\text{Res}_{E_c} \mathbf{G}}^{E_g} := \begin{cases} 0 & \text{if } \frac{1}{2}|\mathbf{G}|^2 \leq E_c \\ (\widehat{V\varphi_{E_c}})_{\mathbf{G}} = (V\varphi_{E_c}, e_{\mathbf{G}}) & \text{if } E_c < \frac{1}{2}|\mathbf{G}|^2 \leq E_g \end{cases}. \quad (\text{A.2})$$

Denote by  $\widehat{\text{Res}_{E_c}}^{E_g} = \left( \widehat{\text{Res}_{E_c} \mathbf{G}}^{E_g} \right)_{\frac{1}{2}|\mathbf{G}|^2 \leq E_g} \in \mathbb{R}^{N_{E_g}}$  with  $N_{E_g}$  the number of planewaves in  $X_{E_g}$ . We can approximate  $A^{-1} \widehat{\text{Res}_{E_c}}$  by  $A^{-1} \widehat{\text{Res}_{E_c}}^{E_g} = \left( A^{-1} \widehat{\text{Res}_{E_c} \mathbf{G}}^{E_g} \right)_{\frac{1}{2}|\mathbf{G}|^2 \leq E_g} \in X_{E_g}(\Omega)$  by solving the linear system

$$A_{E_g} \cdot A^{-1} \widehat{\text{Res}_{E_c}}^{E_g} = \widehat{\text{Res}_{E_c}}^{E_g}, \quad (\text{A.3})$$

where  $A_{E_g} \in \mathbb{R}^{N_{E_g} \times N_{E_g}}$  has the matrix elements  $(A_{E_g})_{ij} = a(e_{\mathbf{G}_i}, e_{\mathbf{G}_j})$ . Using (A.1), (A.2) and (A.3), we therefore approximate the *a posteriori* error indicator  $\eta_{E_c}$  in practical calculations by

$$\eta_{E_c}^{E_g} := \left( \sum_{\mathbf{G} \in \mathbb{L}', \frac{1}{2}|\mathbf{G}|^2 \leq E_g} \widehat{\text{Res}_{E_c} \mathbf{G}}^{E_g} \cdot A^{-1} \widehat{\text{Res}_{E_c} \mathbf{G}}^{E_g} \right)^{\frac{1}{2}}. \quad (\text{A.4})$$

If the potential and eigenfunction are smooth, the approximation error  $|\eta_{E_c} - \eta_{E_c}^{E_g}| \ll \eta_{E_c}$  becomes small for sufficiently large cut-off  $E_g$  [8]. The error indicator  $\eta_{E_c}^{E_g}$  is therefore asymptotically accurate and fully computable. The main cost for computing the estimator comes

from solving the linear system (A.3), which costs  $\mathcal{O}(N_{E_g}^2)$ . Note that if  $E_g$  is proportional to  $E_c$ , the cost for calculating  $\eta_{E_c}^{E_g}$  is  $\mathcal{O}(E_c^d)$ , with  $d$  the dimension of the system.

We further introduce an error estimator with a parameter  $E \in (E_c, E_g)$

$$\eta_{E_c}^{E_g}(E) := \left( \sum_{\mathbf{G} \in \mathcal{R}^*, E_c \leq \frac{1}{2}|\mathbf{G}|^2 \leq E} \widehat{\text{Res}_{E_c}^{E_g} \mathbf{G}} \cdot A^{-1} \widehat{\text{Res}_{E_c}^{E_g} \mathbf{G}} \right)^{1/2}, \quad (\text{A.5})$$

which represents a relatively local error estimator in reciprocal space and is used in Strategy B.

**Remark A.1.** *A natural alternative approach is to construct the a posteriori error estimate by the  $H^{-1}$ -norm of the residual, say  $\|\text{Res}\|_{H^{-1}}$ , as discussed in [11, 12, 13] for Laplace eigenvalue problems. We show in the next subsection that it can be viewed as a first-order perturbation-method-based calculation, and can be improved without too much cost.*

## A.2 A perturbation-based calculation

Solving a linear system to compute the *a posteriori* error estimate may be expensive when the size of the basis becomes large. In this section, we discuss a possible workaround for the computation of the *a posteriori* error estimate based on a perturbation method. Perturbation theory [32] is a classical tool and has been widely used in electronic calculations, e.g. [3, 4, 10]. In particular, [14] provides post-processing algorithms based on a perturbation method which is related to the discussion of this section.

In our construction, we decompose  $A = A_{E_c} + (V - \Pi_{E_c} V \Pi_{E_c})$ , with

$$A_{E_c} = -\Delta + \Pi_{E_c} V \Pi_{E_c}. \quad (\text{A.6})$$

Using a Dyson expansion, we obtain for  $k \geq 1$ ,

$$\begin{aligned} A^{-1} &= \sum_{j=1}^k A_{E_c}^{-1} \left( (\Pi_{E_c} V \Pi_{E_c} - V) A_{E_c}^{-1} \right)^{j-1} + A^{-1} \left( (\Pi_{E_c} V \Pi_{E_c} - V) A_{E_c}^{-1} \right)^k \\ &=: A^{-1,[k]} + A^{-1} \left( (\Pi_{E_c} V \Pi_{E_c} - V) A_{E_c}^{-1} \right)^k, \end{aligned} \quad (\text{A.7})$$

with  $A^{-1,[k]} = \sum_{j=1}^k A_{E_c}^{-1} \left( (\Pi_{E_c} V \Pi_{E_c} - V) A_{E_c}^{-1} \right)^{j-1}$ . Note that the remainder term  $A^{-1} \left( (\Pi_{E_c} V \Pi_{E_c} - V) A_{E_c}^{-1} \right)^k$  will quickly become small if  $\|(\Pi_{E_c} V \Pi_{E_c} - V) A_{E_c}^{-1}\| \ll 1$ . We then approximate the error indicator (A.1) by

$$\eta_{E_c}^{[k]} := \langle \text{Res}_{E_c}, A^{-1,[k]} \text{Res}_{E_c} \rangle_{H', H}^{\frac{1}{2}}, \quad (\text{A.8})$$

replacing  $A^{-1}$  in (A.1) by  $A^{-1,[k]}$ . In practice, we shall perform the above calculations in  $X_{E_g}(\Omega)$ , and use the following *a posteriori* error indicator with  $k = 1, 2$ .

$$\eta_{E_c}^{E_g,[k]} := \left( \sum_{\mathbf{G} \in \mathbb{L}', E_c \leq \frac{1}{2}|\mathbf{G}|^2 \leq E_g} \widehat{\text{Res}_{E_c}^{E_g} \mathbf{G}} \cdot A^{-1,[k]} \widehat{\text{Res}_{E_c}^{E_g} \mathbf{G}} \right)^{\frac{1}{2}}. \quad (\text{A.9})$$

The low computational cost of this estimate comes from the following observation [10]: the operator  $A_{E_c}$  being block diagonal on  $X_{E_c}$  and  $X_{E_c}^\perp$ , with only the Laplace operator which is diagonal in planewaves on  $X_{E_c}^\perp$ , and the residual (A.2) vanishing on  $X_{E_c}$ , the Fourier coefficients of  $A_{E_c}^{-1}\text{Res}_{E_c}$  can be easily evaluated by

$$\widehat{A_{E_c}^{-1}\text{Res}_{E_c}\mathbf{G}}^{E_g} = \frac{\widehat{\text{Res}_{E_c}\mathbf{G}}^{E_g}}{|\mathbf{G}|^2}$$

Therefore the estimator can be computed without solving a linear system (A.3), and the computational cost of (A.9) for  $k = 1$  and  $k = 2$  are now reduced to  $\mathcal{O}(E_g^{d/2})$ . Note that for  $k \geq 3$ , the above structure for convenient evaluation will be destroyed.

Finally, we define the corresponding error estimator with a parameter  $E \in (E_c, E_g)$

$$\eta_{E_c}^{E_g, [k]}(E) := \left( \sum_{\mathbf{G} \in \mathbb{L}', E_c \leq \frac{1}{2}|\mathbf{G}|^2 \leq E} \widehat{\text{Res}_{E_c}\mathbf{G}}^{E_g} \cdot \widehat{A^{-1, [k]}\text{Res}_{E_c}\mathbf{G}}^{E_g} \right)^{\frac{1}{2}}. \quad (\text{A.10})$$

## Appendix B The PAW method

In this section, we introduce the theoretical framework of the PAW method [7, 27, 35], which is one of the most important electronic structure calculation methods used nowadays. The PAW Kohn–Sham model is based on a linear transformation from the smooth pseudo (PS) wave-function  $\varphi_i$  to the real all-electron (AE) wave-function  $\varphi_i^{\text{AE}}$  defined as

$$\varphi_i^{\text{AE}}(\mathbf{r}) = \varphi_i(\mathbf{r}) + \sum_{I=1}^{N_{\text{atom}}} \sum_n (p_n^I, \varphi_i) [\psi_n^I(\mathbf{r}) - \phi_n^I(\mathbf{r})], \quad (\text{B.1})$$

where  $\psi_n^I$ ,  $\phi_n^I$ , and  $p_n^I$  are atomic quantities called AE partial waves, PS partial waves, and projector functions, respectively, and for a given atomic index  $I$ , the index  $n$  runs over the angular momentum and an additional index labeling different partial waves for the same angular momentum. The AE partial wave  $\psi_n^I$  is constructed to be identical to the associated PS partial wave  $\phi_n^I$  outside the radius of the core region  $\Omega_I$  enclosing the atomic position, and the projector functions  $p_n^I$  fulfill

$$\int_{\Omega_I} [p_n^I(\mathbf{r})]^* \phi_m^I(\mathbf{r}) d\mathbf{r} = \delta_{nm} \quad \text{for any } n, m. \quad (\text{B.2})$$

Based on the PAW transformation, one can derive consistent decomposition expressions for the electron density, the kinetic energy of electrons, and the Hartree and the exchange-correlation energy functionals, and then obtain the PAW Hamiltonian by taking variation of the total energy functional with respect to the pseudo density operator.

The AE valence density  $\rho$  is decomposed as

$$\rho(\mathbf{r}) = \tilde{\rho}(\mathbf{r}) + \sum_I [\rho_I^1(\mathbf{r}) - \tilde{\rho}_I^1(\mathbf{r})], \quad (\text{B.3})$$



where  $\tilde{\rho}(\mathbf{r}) = \sum_{i=1}^{N_b} f_i |\varphi_i(\mathbf{r})|^2$ , and

$$\rho_I^1(\mathbf{r}) = \sum_{i=1}^{N_b} \sum_{n,m} f_i(\varphi_i, p_n^I)(p_m^I, \varphi_i) [\psi_n^I(\mathbf{r})]^* \psi_m^I(\mathbf{r}), \quad (\text{B.4})$$

$$\tilde{\rho}_I^1(\mathbf{r}) = \sum_{i=1}^{N_b} \sum_{n,m} f_i(\varphi_i, p_n^I)(p_m^I, \varphi_i) [\phi_n^I(\mathbf{r})]^* \phi_m^I(\mathbf{r}). \quad (\text{B.5})$$

In the derivation of the Hartree and the exchange-correlation functionals, the so-called pseudized core charge  $\tilde{\rho}_{Zc}$ , partial electronic core charge  $\tilde{\rho}_c$ , and compensation charge  $\hat{\rho}$  need to be further introduced. In particular, the compensation charge  $\hat{\rho} = \sum_I \hat{\rho}_I$  and

$$\hat{\rho}_I(\mathbf{r}) = \sum_{i=1}^{N_b} \sum_{n,m} \sum_{L,M} f_i(\varphi_i, p_n^I)(p_m^I, \varphi_i) \hat{Q}_{nm}^{LM,I}(\mathbf{r}), \quad (\text{B.6})$$

where  $\hat{Q}_{nm}^{LM,I}(\mathbf{r})$  are confined in each augmentation region. We refer the readers to [7, 27, 35] for the detailed explanation of these terms.

Finally, the Kohn–Sham equation in the PAW formulation is

$$H[\rho]\varphi_i = \lambda_i S\varphi_i \quad i = 1, \dots, N_b \quad (\text{B.7})$$

with the Hamiltonian  $H[\rho]$  and overlap operator  $S$  detailed below. The PAW Hamiltonian is

$$H[\rho] = -\frac{1}{2}\Delta + \tilde{v}_{\text{eff}} + v_{\text{nl}}, \quad (\text{B.8})$$

where the local potential is given by

$$\tilde{v}_{\text{eff}}[\tilde{\rho}, \hat{\rho}](\mathbf{r}) = v_{\text{H}}[\tilde{\rho} + \hat{\rho} + \tilde{\rho}_{Zc}](\mathbf{r}) + v_{\text{xc}}[\tilde{\rho} + \hat{\rho} + \tilde{\rho}_c](\mathbf{r}), \quad (\text{B.9})$$

and the non-local part is given by

$$(v_{\text{nl}}\varphi_i)(\mathbf{r}) = \sum_I \sum_{n,m} D_{nm}^I(p_m^I, \varphi_i) p_n^I(\mathbf{r}), \quad (\text{B.10})$$

in which the non-local strength  $D_{nm}^I = \hat{D}_{nm}^I + D_{nm}^{1,I} - \tilde{D}_{nm}^{1,I}$  and

$$\hat{D}_{nm}^I = \sum_{L,M} \int_{\Omega_I} \tilde{v}_{\text{eff}}(\mathbf{r}) \hat{Q}_{nm}^{LM,I}(\mathbf{r}) d\mathbf{r}, \quad (\text{B.11})$$

$$D_{nm}^{1,I} = -\frac{1}{2} \int_{\Omega_I} [\psi_n^I(\mathbf{r})]^* [\Delta \psi_m^I(\mathbf{r})] d\mathbf{r} + \int_{\Omega_I} [\psi_n^I(\mathbf{r})]^* \psi_m^I(\mathbf{r}) v_{\text{eff}}^{1,I}(\mathbf{r}) d\mathbf{r}, \quad (\text{B.12})$$

$$\begin{aligned} \tilde{D}_{nm}^{1,I} = & -\frac{1}{2} \int_{\Omega_I} [\phi_n^I(\mathbf{r})]^* [\Delta \phi_m^I(\mathbf{r})] d\mathbf{r} + \int_{\Omega_I} [\phi_n^I(\mathbf{r})]^* \phi_m^I(\mathbf{r}) \tilde{v}_{\text{eff}}^{1,I}(\mathbf{r}) d\mathbf{r} \\ & + \sum_{L,M} \int_{\Omega_I} \tilde{v}_{\text{eff}}^{1,I}(\mathbf{r}) \hat{Q}_{nm}^{LM,I}(\mathbf{r}) d\mathbf{r}, \end{aligned} \quad (\text{B.13})$$

with on-site potentials

$$v_{\text{eff}}^{1,I}[\rho_I^1](\mathbf{r}) = v_{\text{H}}[\rho_I^1 + \rho_{Zc}^I](\mathbf{r}) + v_{\text{xc}}[\rho_I^1 + \rho_c^I](\mathbf{r}), \quad (\text{B.14})$$

$$\tilde{v}_{\text{eff}}^{1,I}[\tilde{\rho}_I^1, \hat{\rho}_I](\mathbf{r}) = v_{\text{H}}[\tilde{\rho}_I^1 + \hat{\rho}_I + \tilde{\rho}_{Zc}^I](\mathbf{r}) + v_{\text{xc}}[\tilde{\rho}_I^1 + \hat{\rho}_I + \tilde{\rho}_c^I](\mathbf{r}). \quad (\text{B.15})$$

Finally, the overlap operator in (B.7) is given by

$$(S\varphi_i)(\mathbf{r}) = \varphi_i(\mathbf{r}) + \sum_I \sum_{n,m} q_{nm}^I(p_m^I, \varphi_i) p_n^I(\mathbf{r}), \quad (\text{B.16})$$

where

$$q_{nm}^I = \int_{\Omega_I} \left\{ [\psi_n^I(\mathbf{r})]^* \psi_m^I(\mathbf{r}) - [\phi_n^I(\mathbf{r})]^* \phi_m^I(\mathbf{r}) \right\} d\mathbf{r}. \quad (\text{B.17})$$

When replacing the standard Kohn–Sham equation (4.1) with the PAW formulation (B.7), the framework of the adaptive algorithm designed in this paper stays the same, though a lot of attention needs to be paid for numerical implementations of the above terms.

## References

- [1] I. Babuška and J. Osborn. Eigenvalue problems. In: Handbook of Numerical Analysis, Vol. II. North-Holland, Amsterdam, 1991.
- [2] G. Bao, G. Hu, and D. Liu. Numerical solution of the Kohn-Sham equation by finite element methods with an adaptive mesh redistribution technique. J. Sci. Comput., 55:372–391, 05 2013.
- [3] S. Baroni, S. de Gironcoli, A. D. Corso, and P. Giannozzi. Phonons and related crystal properties from density-functional perturbation theory. Rev. Mod. Phys., 73:515–562, 07 2001.
- [4] S. Baroni, P. Giannozzi, and A. Testa. Green’s-function approach to linear response in solids. Phys. Rev. Lett., 58:1861–1864, 06 1987.
- [5] R. Becker and R. Rannacher. An optimal control approach to a posteriori error estimation in finite element methods. Acta Numer., 10:1–102, 2001.
- [6] P. Binev, W. Dahmen, and R. DeVore. Adaptive finite element methods with convergence rates. Numer. Math., 97:219–268, 2004.
- [7] P. E. Blöchl. Projector augmented-wave method. Phys. Rev. B, 50(24):17953–17979, 1994.
- [8] E. Cancès, R. Chakir, and Y. Maday. Numerical analysis of nonlinear eigenvalue problems. J. Sci. Comput., 45:90–117, 2010.
- [9] E. Cancès, R. Chakir, and Y. Maday. Numerical analysis of the planewave discretization of some orbital-free and Kohn-Sham models. ESAIM: M2AN., 46:341–388, 2010.
- [10] E. Cancès, G. Dusson, Y. Maday, B. Stamm, and M. Vohralík. A perturbation-method-based a posteriori estimator for the planewave discretization of nonlinear Schrödinger equations. Comptes Rendus Mathématique, 352:941–946, 2014.
- [11] E. Cancès, G. Dusson, Y. Maday, B. Stamm, and M. Vohralík. Guaranteed and robust a posteriori bounds for laplace eigenvalues and eigenvectors: conforming approximations. SIAM J. Numer. Anal., 55:2228–2254, 2017.
- [12] E. Cancès, G. Dusson, Y. Maday, B. Stamm, and M. Vohralík. Guaranteed and robust a posteriori bounds for laplace eigenvalues and eigenvectors: a unified framework. Numer. Math., 140:1033–1079, 2018.
- [13] E. Cancès, G. Dusson, Y. Maday, B. Stamm, and M. Vohralík. Guaranteed a posteriori bounds for eigenvalues and eigenvectors: multiplicities and clusters. preprint, 2019.

- [14] E. Cancès, Geneviève Dusson, Y. Maday, B. Stamm, and M. Vohralík. A perturbation-method-based post-processing for the planewave discretization of Kohn-Sham models. J. Comput. Phys., 307:446–459, 2016.
- [15] C. Canuto, M. Y. Hussaini, A. Quarteroni, and T. A. Zang. Spectral Methods: Evolution to Complex Geometries and Applications to Fluid Dynamics. Springer-Verlag, Berlin, 2014.
- [16] C. Canuto, R. Nochetto, and M. Verani. Adaptive Fourier-Galerkin methods. Math. Comput., 83:1645–1687, 2014.
- [17] J. M. Cascon, C. Kreuzer, R. H. Nochetto, and K. G. Siebert. Quasi-optimal convergence rate for an adaptive finite element method. SIAM J. Numer. Anal., 46:2524–2550, 2008.
- [18] H. Chen, X. Dai, X. Gong, L. He, and A. Zhou. Adaptive finite element approximations for Kohn-Sham models. Multi. Model. & Sim., 12:1828–1869, 2014.
- [19] H. Chen, X. Gong, L. He, Z. Yang, and A. Zhou. Numerical analysis of finite dimensional approximations of Kohn-Sham models. Adv. Compu. Math., 38:1–32, 2011.
- [20] H. Chen, X. Gong, L. He, and A. Zhou. Finite element approximations of nonlinear eigenvalue problems in quantum physics. Comput. Methods Appl. Mech. Engrg., 200:1846–1865, 2011.
- [21] X. Dai, L. He, and A. Zhou. Convergence rate and quasi-optimal complexity of adaptive finite element computations for multiple eigenvalues. IMA J. Numer. Anal., 35:1934–1977, 10 2012.
- [22] X. Dai, J. Xu, and A. Zhou. Convergence and optimal complexity of adaptive finite element eigenvalue computations. Numer. Math., 110:313–355, 2008.
- [23] W. Dörfler. A convergent adaptive algorithm for Poisson’s equation. SIAM J. Numer. Anal., 33:1106–1124, 1996.
- [24] G. Dusson and Y. Maday. A posteriori analysis of a non-linear Gross-Pitaevskii type eigenvalue problem. IMA J. Numer. Anal., 37:94–137, 2017.
- [25] P. Giannozzi et. al. Quantum Espresso. <https://www.quantum.org>.
- [26] X. Gonze et. al. ABINIT. <https://www.abinit.org/>.
- [27] J. Fang, X. Gao, and H. Song. Implementation of the projector augmented-wave method: The use of atomic datasets in the standard PAW-XML format. Commun. Comput. Phys., 26(4):1196–1223, 2019.
- [28] E. Garau, P. Morin, and C. Zuppa. Convergence of adaptive finite element methods for eigenvalue problems. Math. Models Methods Appl. Sci., 19:721–747, 2009.
- [29] Castep Developers Group. CASTEP. <https://www.castep.org>.
- [30] F. Gygi. Adaptive Riemannian metric for plane-wave electronic-structure calculations. Europhys. Lett., 19:617–622, 1992.
- [31] P. Hohenberg and W. Kohn. Inhomogeneous electron gas. Phys. Rev. B, 136:B864, 1964.
- [32] T. Kato. Perturbation Theory for Linear Operators. Springer-Verlag, Berlin Heidelberg, 1976.
- [33] W. Kohn and L. J. Sham. Self-consistent equations including exchange and correlation effects. Phys. Rev. A, 140:A1133–A1138, 1965.

- [34] G. Kresse and J. Furthmüller. Efficiency of ab-initio total energy calculations for metals and semiconductors using a plane-wave basis set. Comput. Mater. Sci., 6:15–50, 1996.
- [35] G. Kresse and D. Joubert. From ultrasoft pseudopotentials to the projector augmented-wave method. Phys. Rev. B, 59:1758–1775, 1999.
- [36] Kari Laasonen, Alfredo Pasquarello, Roberto Car, Changyol Lee, and David Vanderbilt. Car-Parrinello molecular dynamics with vanderbilt ultrasoft pseudopotentials. Phys. Rev. B, 47(16):10142, 1993.
- [37] R. M. Martin. Electronic Structure: Basic Theory and Practical Methods. Cambridge University Press, 2004.
- [38] M. Methfessel and A. T. Paxton. High-precision sampling for brillouin-zone integration in metals. Physical Review B, 40(6):3616, 1989.
- [39] J.E. Osborn. Spectral approximation for compact operators. Math. Comp., 29:712–725, 1975.
- [40] Y. Pan. Some plane wave methods for first principles electronic structure calculation. PhD thesis, Academy of Mathematics and Systems Science, Chinese Academy of Sciences, 2018.
- [41] M. C. Payne, M. P. Teter, M. P. Allan, T. A. Arias, and J. D. Joannopoulos. Iterative minimization techniques for ab-initio total energy calculations-molecular dynamics and conjugate gradients. Rev. Mod. Phys., 64:1045–1097, 1992.
- [42] J.P. Perdew, K. Burke, and M. Ernzerhof. Generalized gradient approximation made simple. Rev. Rev. Lett., 77:3865–3868, 1996.
- [43] L. P. Pitaevskii and S. Stringari. Bose-Einstein Condensation. Clarendon, Oxford, 2003.
- [44] P. Pulay. Convergence acceleration of iterative sequences: The case of scf iteration. Chem. Phys. Lett., 73:393–398, 1980.
- [45] Y. Saad, J. R. Chelikowsky, and S. M. Shontz. Numerical methods for electronic structure calculations of materials. SIAM Rev., 52:3–54, 2010.
- [46] P. Suryanarayana, V. Gavini, T. Blesgen, K. Bhattacharya, and M. Ortiz. Non-periodic finite-element formulation of Kohn-Sham density functional theory. J. Mech. Phys. Solids, 58:256–280, 2010.
- [47] The VASP team. VASP. <https://www.vasp.at/>.
- [48] E. Tsuchida and M. Tsukada. Adaptive finite-element method for electronic-structure calculations. Phys. Rev. B, 54:7602–7605, 1996.
- [49] David Vanderbilt. Soft self-consistent pseudopotentials in a generalized eigenvalue formalism. Phys. Rev. B, 41(11):7892, 1990.